

Electro-Mechanical Response of a 3D Nerve Bundle Model to Mechanical Loads Leading to Axonal Injury

I. Cinelli, *Student Member, IEEE*, M. Destrade, M. Duffy, *Senior Member, IEEE*, and P. McHugh

Abstract— Axonal damage is one of the most common pathological features of traumatic brain injury, leading to abnormalities in signal propagation for nervous systems. We present a 3D fully coupled electro-mechanical model of a nerve bundle, made with the finite element software Abaqus 6.13-3. The model includes a real-time coupling, modulated threshold for spiking activation and independent alteration of the electrical properties for each 3-layer fibre within the bundle. Compression and tension are simulated to induce damage at the nerve membrane. Changes in strain, stress distribution and neural activity are investigated for myelinated and unmyelinated nerve fibres, by considering the cases of an intact and of a traumatized nerve membrane. Results show greater changes in transmitting action potential in the myelinated fibre.

I. INTRODUCTION

Traumatic brain injury (TBI) is caused by mechanical loading to the head (such as sudden acceleration or a blast wave), causing pathologies which range from focal damage of brain tissue to widespread axonal injury [1], [2].

Axonal damage is one of the most common pathological features of traumatic brain injury. It is classified as diffuse axonal injury (DAI), part of the mild and severe cases of TBI [1], [3] and it is thought to be responsible for long-lasting neurological impairments following TBI [3], [4].

Experimental studies conducted on a single axon [5] and nerve fibres [6] aim to induce axonal injury by applying pressure [7], [8], displacement [1], [6], strain [5], [9], shear strain [10] and electroporation [11]. Although different types of loads seem to initiate DAI, recent studies have shown that the degree of electrophysiological impairment and morphological damage of neural cells is directly related to the magnitude and rate of axonal stretch [1], [5], [6], [12]. Deformation beyond a critical threshold [6] can damage the axonal cytoskeleton, resulting in a loss of membrane integrity and impairment of axoplasmic transport, leading to changes in electrical signal propagation [5], [13].

Multi-scale computational models of traumatic brain injury are used to better understand the impact of macroscale head injury on DAI [1], [2]. Previous modelling efforts have simulated one-dimensional damage of a nerve fibre [2] and two-dimensional axonal injury of brain tissue [1]. However, advanced three-dimensional (3D) models for explaining

injury and changes in propagation at the axonal and bundle levels are still lacking.

This work presents a novel approach for evaluating and quantifying the changes in neural activity due to axonal injury. To address the existing limitations in understanding of the link between TBI and DAI at the microscale level [1], [2], here, a 3D finite element (FE) model of a nerve bundle includes an accurate representation of a nerve cell made of extracellular media (ECM), a membrane and intracellular media (ICM). A series of mechanical loads (such as pressure [7] and displacement [6]) are applied on the bundle to induce a certain level of damage at the nerve membrane of a fibre, altering the fibre activation dynamics and transmission [12], [13].

This model presents a unique framework for investigating the changes of strain and stress distributions on myelinated and unmyelinated nerve fibres and bundles. Here, the neural electrical activity (including piezoelectricity [14] and electrostriction [15]) is directly coupled to its mechanical deformation by using electro-thermal equivalences in FE analysis [16]. Electro-thermal equivalences and equivalent material properties have been shown to provide an efficient approach to resolve 3D electrical problems in a coupled electro-mechanical analysis using the commercial FE code Abaqus CAE 6.13-3 [16].

The electro-mechanical coupling is validated based on the strain-based damage criterion, simulating a shift in the stretch-damaged transient ionic currents of the nerve membrane [2], [12]. Then, the injury threshold takes into account axonal strain along the nerve fibre length only. The strain, in this direction, has been shown to be a physiologically relevant injury criterion for multiscale TBI models [1], [2]. This approach might prove crucial to study the mechanics behind neuro-physiology as observed experimentally in damaged nerve membranes of clinical cases (such as multiple sclerosis) [5], [17], [18].

II. METHODS

A. Electro-Mechanical Coupling

Building on the equivalent electro-thermal modelling approach for nerve cells described in [16], coupling of the electro-mechanical effects of the action potential [19] is achieved through modelling of the nerve membrane as a piezoelectric material [14], [15].

* All the authors are with NUI, Galway (Republic of Ireland).

Emails: i.cinelli@nuigalway.ie; michel.destrade@nuigalway.ie; maeve.duffy@nuigalway.ie; peter.mchugh@nuigalway.ie;

The thermo-elastic strain-stress relation is given in (1), where $\{\varepsilon\}$ is the total strain vector, $[\beta]$ the compliance matrix, $\{\sigma\}$ the mechanical stress, $\{\alpha\}$ is the thermal expansion coefficient vector and ΔT is the temperature difference [20], [21],

$$\{\varepsilon\} = [\beta]\{\sigma\} + \{\alpha\}\Delta T \quad (1)$$

Based on this relation, the piezo-elastic relation is given in Equation (2) where $\{\delta\}$ is the piezoelectric strain coefficient vector, h is the thickness of the piezoelectric layer and ΔV is the voltage difference [20], [21],

$$\{\varepsilon\} = [\beta]\{\sigma\} + \{\delta\}(\Delta V/h) \quad (2)$$

By the electro-thermal analogy [20], [21], the electric field (given by $\Delta V/h$ in (2)) is equivalent to a thermal load, while the piezoelectric constants are equivalent to the thermal expansion coefficients, see (1) and (2). For the case of a nerve membrane, it is assumed that the piezoelectric effect is only relevant in the through-thickness direction, and we thus take only one non-zero component for δ , approximately 1 nm per 100 mV in that direction [14].

B. Model

The nerve bundle model simulates the exchange of charges in four identical neurites. Each neurite consists of a cylindrical region of ICM, see Fig. 1 (e), enclosed by a thin membrane and surrounded by ECM, see Fig. 1 (c) [16]. Two fibre bundle models are used in this study: a fully unmyelinated bundle (UN-FB) and a fully myelinated bundle (MY-FB). The neurite radii are: $a_{ICM} = 0.477 \mu\text{m}$, $a_M = 0.480 \mu\text{m}$ and $a_{ECM} = 0.500 \mu\text{m}$ [16]. As a first step, this analysis is focussed on the radial distribution of charges rather than on the longitudinal variations, hence the length of the bundle is $5 \mu\text{m}$ for a diameter equal to $2.41 \mu\text{m}$ in both cases, see Fig. 1 (a) and (b). The diameter is within the range of the measured diameters of the human optic nerve [22].

Modelling a myelinated fibre, we assume an ICM encased by a single layer, which is periodically-partitioned (axially along the fibre length) similarly to the histologic section of a myelinated fibre, see Fig (d.1) and (d.2). The insulation sheath of myelin around the nerve fibre is modelled as an insulating layer, which replaces the membrane layer at regular intervals along the fibre [23], see Fig.1 (d.1). Different conductivity values are assigned to denote the myelin and membrane sections [23], see Fig. (d.2). The width of the piecewise conductive membrane regions (or Ranvier's nodes) is $0.002 \mu\text{m}$ and the internode distance is $1 \mu\text{m}$ (refers to [23]), see Fig.1 (d.2). The finite element mesh designs were motivated by computational efficiency. Incompressible isotropic mechanical properties [24] are assumed in both models while the electrical model parameters for predicting the basic action potential are taken from [19], with those accounting for dependence on strain taken from [2].

C. Damage evaluation

The strain-based damage affects the sodium and potassium reversal potentials ($E_{Na}(\varepsilon_m)$ and $E_K(\varepsilon_m)$), simulating the changes of the ionic concentration across the nerve membrane depending on the membrane strain (ε_m) [2].

If a maximum value of strain, $\tilde{\varepsilon}$, is exceeded, then the reversal potentials are zero, otherwise the changes follow in (3) if $\varepsilon_m < \tilde{\varepsilon}$ [2]:

$$\begin{cases} E_{Na}(\varepsilon_m) = E_{Na0}(1 - (\varepsilon_m/\tilde{\varepsilon})^\gamma) \\ E_K(\varepsilon_m) = E_{K0}(1 - (\varepsilon_m/\tilde{\varepsilon})^\gamma) \end{cases} \quad (3)$$

Here, the strain threshold is set at 0.21 as an indicator of the onset of functional damage [6]. The parameter γ is an index referring to the sensitivity of the damage for small versus large deformation, see [2]. Additionally, the reversal potential of the leak ions E_{l-} is not influenced by the strain but varies based on changes in gradient concentrations of potassium and sodium across the membrane [2].

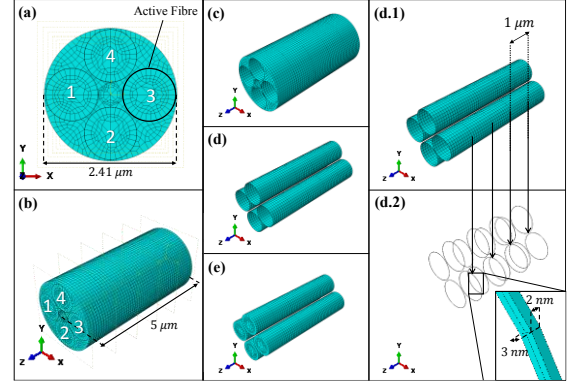


Fig. 1. In (a), frontal view and, in (b), isometric view of the four-fibre nerve bundle, with each fibre made of 3 layers. The model consists of 53,240 nodes, 50,166 coupled thermal-structural (Abaqus C3D8T) elements. Fibre #3 is the active fibre, i.e. the fibre activated by a voltage Gaussian distribution [24]. Fibre #1, #2 and #4 are activated by the charges diffusing from Fibre #3. In (c), the ECM; in (d), the membrane and, in (e), the ICM. In the case of myelinated fibres, the membrane layer is periodically-partitioned (axially along the fibre length) to model the insulation sheath of myelin layer, see (d.1), and the Ranvier's node, see (d.2). The myelin layer length is $1 \mu\text{m}$ and the Ranvier's node length is 2 nm , while the radial thickness of the layer is equal to 3 nm [16], [23].

D. Implementation

The implementation of the coupled Hodgkin and Huxley (HH) model (on the right) is shown in Fig. 2, in contrast to the uncoupled HH model (on the left). By using the electro-thermal equivalence implementation of the neural activity, the distribution of voltage and currents can be seen in 3D by using well established coupled thermo-mechanical software simulation tools. In the coupled model, the membrane electrical conductivity changes in response to the membrane voltage and strain [2], [19], while the electrical capacitance per unit area changes with the square of the voltage [25]. The HH resting voltage potentials are changing due to the strain at the membrane [2], [12], hence the threshold of spike initiation changes as in [19]. The model is implemented as a coupled thermo-mechanical model in Abaqus CAE by using user-defined subroutines to assign thermal equivalent electrical properties to the membrane of each fibre, independently, based on the spike initiation [26], strain [2], [12] and voltage [25] generated at the same membrane.

E. Boundary Conditions

A voltage Gaussian distribution activates Fibre #3 generating a flow of ionic currents across its membrane [19], see Fig. 2, while the other fibres are activated only if the diffused charges from Fibre #3 generate an input voltage

higher than the modulated threshold [26]. The 3D distribution of charges on Fibre #3 modulates the activation of the other fibres. In the first case, an instantaneous uniform compression is applied to the bundle to simulate injury conditions due to mild (less than $55kPa$), moderate ($55 - 95 kPa$) and severe (higher than $95 kPa$) pressure [7]. The case of extreme pressure ($1GPa$) is also considered. In the second case, three values of instantaneous uniform stretch have been applied as displacement boundary conditions to simulate 14%, 21% and 34% of total deformation [6].

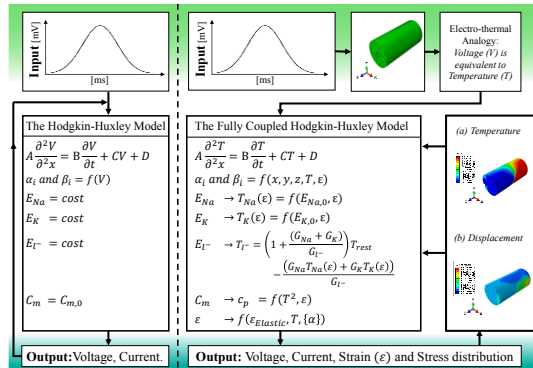


Fig. 2. Flowchart of the code describing the active behaviour of the nerve's membrane: on the left the HH dynamics [19] and on the right the fully coupled HH dynamics. By using electro-thermal equivalences, the HH dynamics is implemented as an equivalent thermal process, in which the membrane's conductivity changes as in [19] and the capacitance, C_m , changes as in [25]. The HH parameters are changing based on the temperature, T , and strain, ϵ , at the membrane [2]. The strains generated in the model are a function of temperature and thermal expansion coefficients, $\{\alpha\}$, see (1) and (2). Voltage, current, strain and stresses distribution are only a few of the 3D results released by Abaqus.

F. Validation

As in [2], [12], the strain-based damage evaluation criterion refers to a traumatic mechanically-induced damage on a nerve fibre (refer to [2], [12]). This is validated by shifting up the resting ionic potentials of the HH model by $20 mV$, simulating experimental evidence of damaged nerve fibres [12], [13], as in [2]. This is called the coupled left-shift (LS) model of the HH model [12]. Only a fraction of nodal channels affected (AC) by the damage undergoes a LS , while the rest of the membrane's channel, $(1 - AC)$, remains intact [12]. Here, only the extreme cases of entire membrane traumatized ($AC = 1$) or intact membrane ($AC = 0$) are shown.

III. RESULTS

In Fig. 3 the hyperpolarization of an unmyelinated bundle due to applied pressure levels, P , simulating mild to severe pressure inducing DAI [7], are shown. Similarly, Fig. 4 (a) and Fig. 4 (b) show the radial displacement at Fibre #3 of an unmyelinated and myelinated bundle for the same pressure values [7]. In contrast to the reference case of an intact nerve cell ($P = 0 kPa$ and $AC = 0$), see Fig. 3, the action potential, in both unmyelinated and myelinated bundles, is delayed by about $4.70 msec$ and $16.2 msec$ for the extreme pressure case and the mild-severe case [7], respectively, although the fibre are activated at the same time in all the cases. In a first investigation, the resting voltage potentials are changed due

to the induced-deformation in the bundle and the magnitude of the action potential is, hence, reduced [2], see Fig. 3. Higher reduction is found in a compressed unmyelinated bundle than in a myelinated one. Differences between intact and traumatized nerve membranes ($AC = 0$ versus $AC = 1$) are very small when mild-severe pressures are applied. Hence, only the case of an intact nerve membrane is shown in Fig. 3. An extreme pressure leads to both a reduction in magnitude and an increase of the voltage baseline up to $-24 mV$ for an intact membrane and up to $-7mV$ for a traumatized membrane, see Fig. 3, with $C = 0$ and $AC = 1$.

This model shows greater radial displacement of the membrane in an unmyelinated fibre than in a myelinated fibre for pressure levels up to $65 kPa$, see Fig. 4. The myelin layer constrains the deformation of the Ranvier's nodes, which are the only regions throughout the fibre to show voltage-induced membrane displacement [14], see Fig. 4 (b). However, in the case of severe pressure ($192 kPa$), the magnitude of displacement is greater over the length of a myelinated fibre than an unmyelinated one, see Fig. 4. An unmyelinated layer displaces according to the charges exchanged across the nerve membrane, see Fig. 4 (a). For the cases of mild to severe pressure, the displacement peak varies from $-0.504 \mu m$ to $-1.22 \mu m$, respectively, see Fig. 4 (a). Because of the myelin layer, the charge-induced displacement of a myelinated fibre is less than in the previous case (see Fig. 4 (b)) and it displaces according to the loading condition, see Fig. 4 (b). The myelin layer does not have the same piezoelectric properties of the membrane, hence, it constrains the membrane deformations. In Fig. 4, the displacement at the membrane under an extreme pressure follows the loading condition applied, here it is not shown.

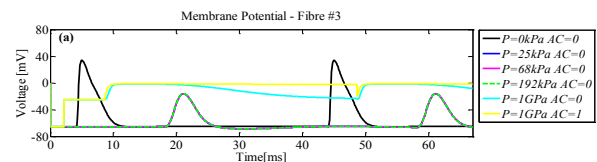


Fig. 3. Voltage [mV] of an unmyelinated bundle under mild ($25kPa$), moderate ($68kPa$) and severe ($192kPa$) pressure [7]. Similar results are found for the Ranvier's node regions of the myelinated fibres. AC is the fraction of affected ionic channels by the strain: $AC = 0$ is for an intact membrane and $AC = 1$ for a traumatized membrane [12]. Data are the maximum radial displacement of a node on Fibre #3. Similar membrane voltage changes are found for 25 – 192 kPa with $AC = 1$

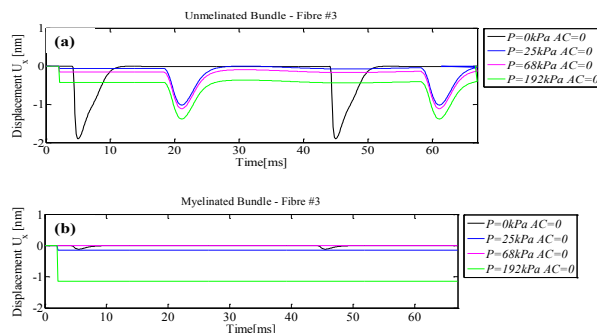


Fig. 4. Displacement [nm] of an unmyelinated, (a), and myelinated bundle, (b), under mild ($25kPa$), moderate ($68kPa$) and severe ($192kPa$) pressure [7]. AC is the fraction of affected ionic channels by the strain: $AC = 0$ is for an intact membrane and $AC = 1$ for a traumatized membrane [12]. Data are the maximum radial displacement of a node on Fibre #3.

The second investigation of tension conditions reproduce the uni-axial test in [6]. An elongation L equal to $0.7 \mu\text{m}$, $1.05 \mu\text{m}$ and $1.7 \mu\text{m}$ simulates 5%, 14% and 34% of stretch, respectively [7]. A 34% deformation simulates the case of anode break excitation [19] in both types of fibre (not shown here). In an unmyelinated bundle, the voltage baseline is shifted up to -24 mV for 14% stretch, while the peak is approximately -2 mV , see Fig. 5 (a). If the membrane is traumatized, the action potential is a signal with constant magnitude of approximately -2 mV , respectively, see Fig. 5 (a). A 14% stretch shift the voltage baseline up to -61 mV . However, the peak is approximately reduced to -10 mV and -20 mV with $AC = 0$ and $AC = 1$, respectively, see Fig. 5(a). In contrast, in a myelinated bundle, see Fig. 5(b), slight differences have been found between intact and traumatized membranes. Here, the peak of the action potential is approx. -34 mV and -53 mV , for 5% and 14% of applied stretch, see Fig. 5(b). Lower current density at the Ranvier's nodes is mainly due to the higher localized strain.

IV. CONCLUSION

Electrophysiological impairments of axonal injury due to sudden DAI-induced pressures reduce the peak of the action potential by approximately 50 mV , while elongation tests reduce it by approximately 30 mV in unmyelinated bundles and by approximately 80 mV in myelinated bundles. In general, the signal seems to be affected more in myelinated fibres due to the myelin layer around the fibre. Future investigations will clarify the impact of different rates of deformation in mechanical loadings [1], [2], and will investigate the interaction between neighbouring fibres within a 3D nerve bundle.

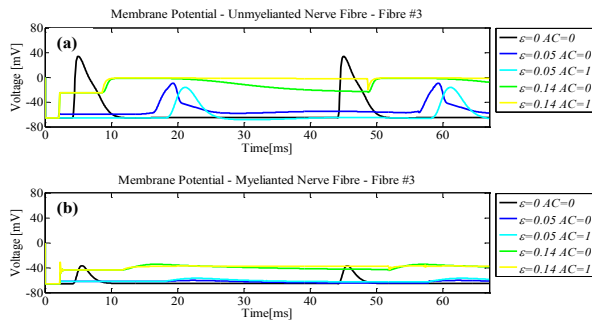


Fig. 5. The $5 \mu\text{m}$ bundle is elongated by $0.7 \mu\text{m}$ and $1.05 \mu\text{m}$ [6]. In (a) and in (b) the membrane's potential of an unmyelinated and myelinated bundle respectively. Data are the maximum radial displacement of a node on Fibre #3.

ACKNOWLEDGMENT

The authors gratefully acknowledge funding from the Galway University Foundation, the Biomechanics Research Centre and the Power Electronics Research Centre, College of Engineering and Informatics, National University of Ireland Galway.

REFERENCES

[1] R. M. Wright and K. T. Ramesh, "An axonal strain injury criterion for traumatic brain injury," *Biomech. Model. Mechanobiol.*, vol. 11, no. 1–2, pp. 245–260, 2012.

[2] A. Jérusalem, J. A. García-Grajales, A. Merchán-Pérez, and J. M. Peña, "A computational model coupling mechanics and electrophysiology in spinal cord injury," *Biomech. Model. Mechanobiol.*, vol. 13, no. 4, pp. 883–896, 2014.

[3] D. H. Smith and D. F. Meaney, "Axonal damage in traumatic brain injury," *Prog Clin Neurosci*, vol. 6, no. 6, pp. 483–492, 2000.

[4] H. C. Wang and Y. Bin Ma, "Experimental models of traumatic axonal injury," *J. Clin. Neurosci.*, vol. 17, no. 2, pp. 157–162, 2010.

[5] J. a Galbraith, L. E. Thibault, and D. R. Matteson, "Mechanical and electrical responses of the squid giant axon to simple elongation," *J. Biomech. Eng.*, vol. 115, no. 1, pp. 13–22, 1993.

[6] A. C. Bain and D. F. Meaney, "Tissue-level thresholds for axonal damage in an experimental model of central nervous system white matter injury," *J. Biomech. Eng.*, vol. 122, no. 6, pp. 615–622, 2000.

[7] S. Hosmane, A. Fournier, R. Wright, L. Rajbhandari, R. Siddique, I. H. Yang, K. T. Ramesh, A. Venkatesan, and N. Thakor, "Valve-based microfluidic compression platform: single axon injury and regrowth," *Lab Chip*, vol. 11, no. 22, p. 3888, 2011.

[8] P. E. Gallant, "The direct effects of graded axonal compression on axoplasm and fast axoplasmic transport," *J. Neuropathol. Exp. Neurol.*, vol. 51, no. 2, pp. 220–30, 1992.

[9] R. Shi and J. Whitebone, "Conduction deficits and membrane disruption of spinal cord axons as a function of magnitude and rate of strain," *J. Neurophysiol.*, vol. 95, no. 6, pp. 3384–90, 2006.

[10] M. C. LaPlaca, D. K. Cullen, J. J. McLoughlin, and R. S. Cargill, "High rate shear strain of three-dimensional neural cell cultures: A new in vitro traumatic brain injury model," *J. Biomech.*, vol. 38, no. 5, pp. 1093–1105, 2005.

[11] P. E. Gallant and J. A. Galbraith, "Axonal structure and function after axolemmal leakage in the squid giant axon," *J Neurotrauma*, vol. 14, no. 11, pp. 811–822, 1997.

[12] P. A. Boucher, B. Joós, and C. E. Morris, "Coupled left-shift of Nav channels: Modeling the Na⁺-loading and dysfunctional excitability of damaged axons," *J. Comput. Neurosci.*, vol. 33, no. 2, pp. 301–319, 2012.

[13] N. Yu, C. E. Morris, B. Joós, and A. Longtin, "Spontaneous Excitation Patterns Computed for Axons with Injury-like Impairments of Sodium Channels and Na/K Pumps," *PLoS Comput. Biol.*, vol. 8, no. 9, 2012.

[14] P.-C. Zhang, A. M. Keleshian, and F. Sachs, "Voltage-induced membrane movement," *Nature*, vol. 413, no. 6854, pp. 428–432, 2001.

[15] L. D. Mosgaard, K. a. Zecchi, and T. Heimburg, "Mechano-capacitive properties of polarized membranes," *Soft Matter*, vol. 11, no. 40, pp. 7899–7910, 2015.

[16] I. Cinelli, M. Duffy, and P. E. McHugh, "Thermo-electrical equivalents for simulating the electro-mechanical behavior of biological tissue," in *2015 37th Annual International Conference of the IEEE Engineering in Medicine and Biology Society (EMBC)*, 2015, pp. 3969–3972.

[17] C. Demerens, B. Stankoff, M. Logak, P. Anglade, B. Allinquant, F. Couraud, B. Zalc, and C. Lubetzki, "Induction of myelination in the central nervous system by electrical activity," *Proc. Natl. Acad. Sci. U. S. A.*, vol. 93, no. 18, pp. 9887–9892, 1996.

[18] D. M. Geddes, R. S. Cargill, and M. C. LaPlaca, "Mechanical stretch to neurons results in a strain rate and magnitude-dependent increase in plasma membrane permeability," *J. Neurotrauma*, vol. 20, no. 10, pp. 1039–1049, 2003.

[19] A. L. Hodgkin and A. F. Huxley, "A Quantitative Description Of Membrane Current And Its Application To Conduction And Excitation In Nerve," *J. Physiol.*, vol. 117, pp. 500–544, 1952.

[20] S. A. Tawfik, D. Stefan Dancila, and E. Armanios, "Unsymmetric composite laminates morphing via piezoelectric actuators," *Compos. Part A Appl. Sci. Manuf.*, vol. 42, no. 7, pp. 748–756, 2011.

[21] M. Staworko and T. Uhl, "Modeling and simulation of piezoelectric elements - comparison of available methods and tools," *Mechanics*, vol. 27, no. 4, pp. 161–171, 2008.

[22] J. a Perge, J. E. Niven, E. Mugnaini, V. Balasubramanian, and P. Sterling, "Why do axons differ in caliber?," *J. Neurosci.*, vol. 32, no. 2, pp. 626–638, 2012.

[23] P. D. Einziger, L. M. Livshitz, a. Dolgin, and J. Mizrahi, "Novel cable equation model for myelinated nerve fiber," *First Int. IEEE EMBS Conf. Neural Eng. 2003. Conf. Proceedings.*, vol. 52, no. 10, pp. 1632–1642, 2003.

[24] A. El Hady and B. B. Machta, "Mechanical surface waves accompany action potential propagation," *Nat. Commun.*, vol. 6, no. 6697, p. 6697, 2015.

[25] O. Alvarez and R. Latorre, "Voltage-dependent capacitance in lipid bilayers made from monolayers," *Biophys. J.*, vol. 21, no. 1, pp. 1–17, 1978.

[26] J. Platkiewicz and R. Brette, "A threshold equation for action potential initiation," *PLoS Comput. Biol.*, vol. 6, no. 7, p. 25, 2010.